JOC The Journal of Organic Chemistry

Article

pubs.acs.org/joc

Triazole-Linked Anthracenyl-Appended Calix[4]arene Conjugate As Receptor for Co(II): Synthesis, Spectroscopy, Microscopy, and Computational Studies

V. V. Sreenivasu Mummidivarapu,[†] Vijaya Kumar Hinge,[‡] Khatija Tabbasum,[†] Rajesh G. Gonnade,[§] and Chebrolu P. Rao*[,†,‡]

[†]Department of Chemistry and [‡]Department of Biosciences and Bioengineering, Indian Institute of Technology Bombay, Powai, Mumbai 400 076, India

[§]Center for Materials Characterization, National Chemical Laboratory, Pune 411 008, India

Supporting Information

ABSTRACT: A new triazole-linked anthracenyl-appended calix[4]arene-1,3-diconjugate (**L**) has been synthesized and characterized, and its single crystal XRD structure has been established. Binding properties of **L** toward different biologically relevant metal ions have been studied by fluorescence and absorption spectroscopy in ethanol. **L** exhibits selective recognition of Co^{2+} and can detect down to a concentration of 55 ppb (0.92 μM). The roles of the calix[4]arene platform as well as the preorganized binding core in **L**'s selective recognition have been demonstrated by studying appropriate control molecules. The mode of binding of **L** with Co^{2+} has been modeled both by DFT and MD computational calculations. **L** and its Co^{2+} complex could be differentiated on the basis of the nanostructural features observed in AFM and TEM.

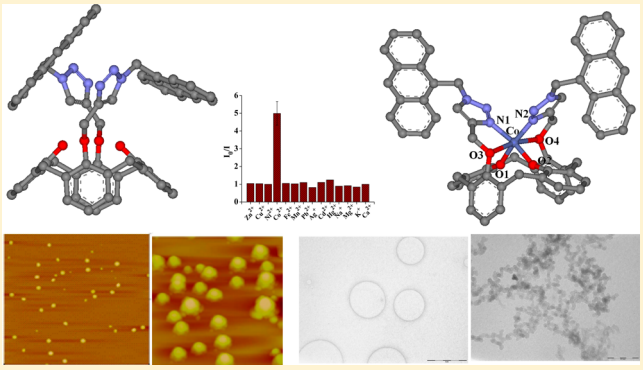

INTRODUCTION

Cobalt is one of the most essential micronutrients and is present in about 0.3 mg/L concentration in ocean water. The ~1.5 mg that is present in an adult human body is distributed in the liver, kidney, and bone.[1] Cobalt also plays important role in the metabolism of iron and thereby in the synthesis of hemoglobin.[2] It is an essential trace element found in the cobalamin coenzyme (vitamin B_{12}) associated with a number of enzymes.[3] Deficiency of cobalt may cause anemia, retarded growth, and loss of appetite.[1b,4] In large doses, cobalt salts can be toxic.[5] There is an increased interest in studying cobalt in environmental and biological samples. Thus the development of synthetic receptors for the selective recognition of cobalt continues to intrigue researchers. Although there are a few small molecular chemosensors for Co^{2+} in the literature, there is only one in the case of calix[4]arene.[6] In this regard, we report the synthesis, characterization, and metal ion binding studies of a 1,3-diderivative of calix[4]arene appended to anthracenyl moiety through a triazole linker and its selectivity toward Co^{2+}.

RESULTS AND DISCUSSION

The receptor molecule **L** was synthesized in two steps (Scheme 1) starting from *p-tert*-butylcalix[4]arene, **P** by reacting with propargyl bromide to form a dipropargyl, $\mathbf{P_2}$. Reaction of $\mathbf{P_2}$ with 9-(azidomethyl) anthracene ($\mathbf{P_1}$) results in the formation of **L**. In turn, the 9-(azidomethyl) anthracene was synthesized from 9-chloromethyl anthracene. A single strand analogue devoid of the calix[4]arene platform, $\mathbf{L_1}$ has been synthesized by two steps starting from *p-tert*-butylphenol instead of *p-tert*-butyl-calix[4]arene.[7]

$\mathbf{P_1}$, $\mathbf{P_2}$, $\mathbf{L_1}$, and **L** were well characterized by ^{1}H, ^{13}C nuclear magnetic resonance (NMR), Fourier transform infrared spectroscopy (FTIR), and high resolution mass spectrometry (HRMS) (Experimental Section and Supporting Information S1−S4). ^{1}H NMR spectrum of **L** supported the presence of cone conformation as can be noticed from the appearance of peaks at 2.82 and 3.61 ppm for the bridge -CH_2 moiety. The cone conformation has been further confirmed from the structure determined on the basis of single crystal X-ray diffraction (XRD) as reported in this paper. On the other hand, the two -CH_2 groups, viz., the one attached to the anthracenyl moiety and the other one attached to the lower rim 'O' were identified as 6.46 ppm {cross peak (i)} and 4.80 ppm {cross peak (ii)} could be differentiated from the heteronuclear single quantum correlation (HSQC) spectra (Figure 1).

Single Crystal X-ray Structure of the Receptor Molecule. Single crystals of the receptor were obtained from

Received: January 8, 2013
Published: March 19, 2013

Scheme 1. Synthesis of L[a]

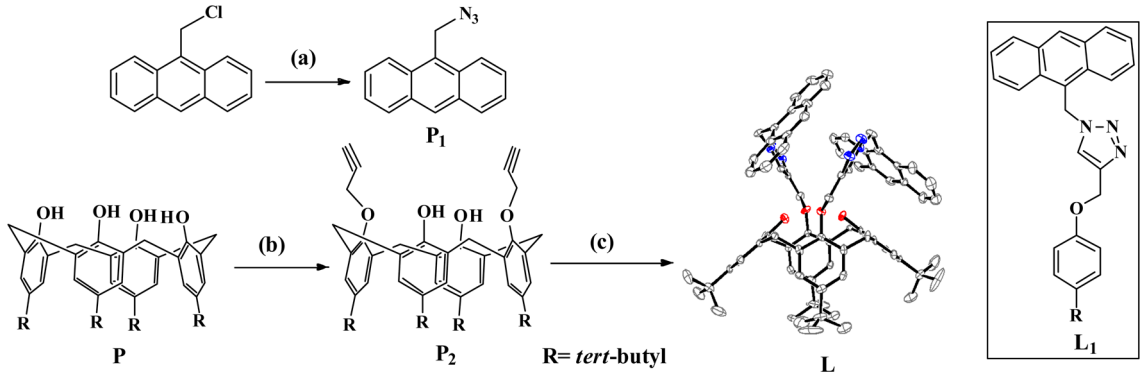

[a](a) NaN_3, DMF; (b) K_2CO_3, propargyl bromide, dry acetone, 16 h; (c) P_1, $CuSO_4 \cdot 5H_2O$, sodium ascorbate, {dichloromethane (5 mL) + *tert*-butanol (5 mL) + water (10 mL)}, 24 h. L_1 is a control molecule without the calix[4]arene platform.

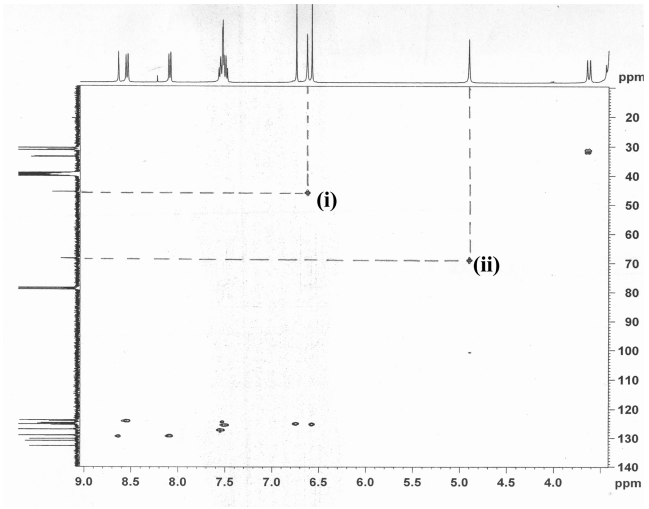

Figure 1. HSQC ($^1H-^{13}C$) spectra for **L** in DMSO-d_6.

slow evaporation of a solution of **L** dissolved in $CHCl_3$, and these were found to be triclinic with $P\bar{1}$ space group (Supporting Information, Table S1). The single crystal XRD structure of **L** exhibits cone conformation for the calixarene by retaining two intrarim O–H···O hydrogen bonds with O···O distance of 2.34 Å at the lower rim (Figure 2a). The distance between the two phenolic oxygens at the lower rim is 3.29 Å, and the distance between the centroid of the phenyl to the centroid of the anthracene moiety is 4.50 Å. The circular hydrogen bonding stabilizes the **L** in cone conformation and was confirmed by the ^1H NMR studies. The $\pi\cdots\pi$ interactions present between the neighbor anthracene units can be seen from the packing of molecules in the lattice. The distance between the centroids of two anthracenyl moieties is 4.18 Å (Figure 2b). A metal ion binding core of N_2O_4 is present in **L**, and the preorganized binding core can interact with the incoming metal ion. The stereoview shows that while one of the anthracenyl moiety is bent inward, the other is bent outward with respect to the calix[4]arene platform (Supporting Information, S5).

Fluorescence Titration Studies of L with M^{2+} in Ethanol. The ion recognition of **L** has been studied by exciting the corresponding solutions at 368 nm and measuring the emission in the 378–550 nm range. Thus, among Na^+, K^+, Mg^{2+}, Ca^{2+}, Mn^{2+}, Fe^{2+}, Co^{2+}, Ni^{2+}, Cu^{2+}, Zn^{2+}, Cd^{2+}, Ag^+, and Hg^{2+} ions studied, only Co^{2+} exhibited fluorescence quenching upon titration with **L**. As the concentration of Co^{2+} increases, the fluorescence intensity of 417 nm band decreases by an extent of ~5 ± 1 fold (Figure 3, Supporting Information, S6). The minimum concentration at which **L** can detect Co^{2+} was obtained from a dilution experiment carried out by keeping the mole ratio of **L** and Co^{2+} as 1:1 and was found to be 55 ppb (0.92 μM) (Supporting Information, S7). The quenching constant of **L** by Co^{2+} has been derived by Stern–Volmer equation, and the corresponding quenching constant, K_q, was found to be 476,552 ± 20000 M^{-1} (Supporting Information, S8).

Similar fluorescence studies were carried out with the control molecules such as P_1 and L_1 and found no significant change in the emission intensity, suggesting that a preorganized binding core in **L** is indeed required for such recognition (Figure 4a). The formation of a 1:1 complex was confirmed by ESI MS,

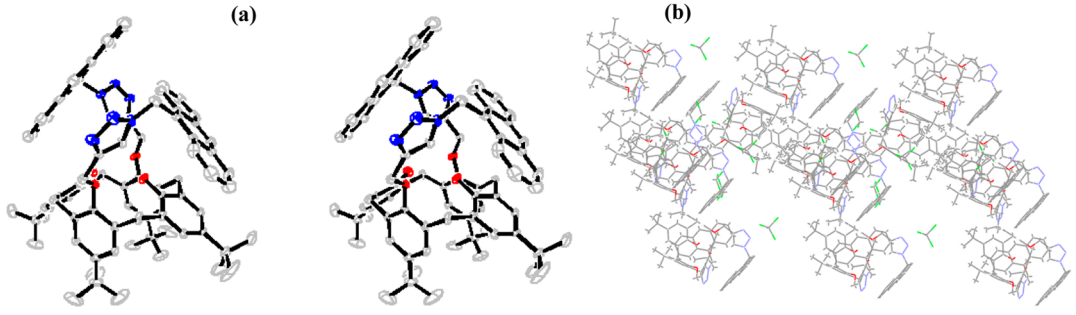

Figure 2. (a) Stereoview of the molecular structure of **L** as obtained from the single crystal XRD. (b) Crystal packing diagram of **L**.

dx.doi.org/10.1021/jo400038x | J. Org. Chem. 2013, 78, 3570–3576

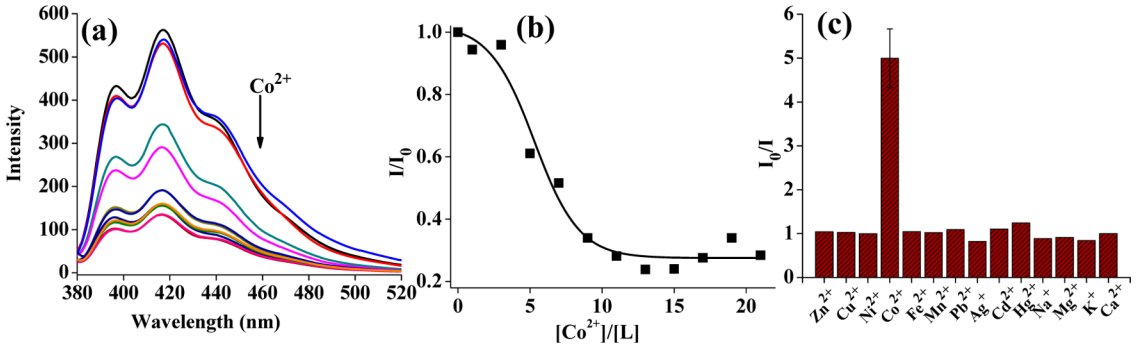

Figure 3. Fluorescence studies of **L** with metal ions: (a) fluorescence spectra obtained during the titration of **L** with Co^{2+} in ethanol (λ_{ex} = 368 nm); (b) fluorescence intensity as a function of $[Co^{2+}]/[L]$ mole ratio; (c) relative fluorescence intensity of **L** in the presence of different metal ions.

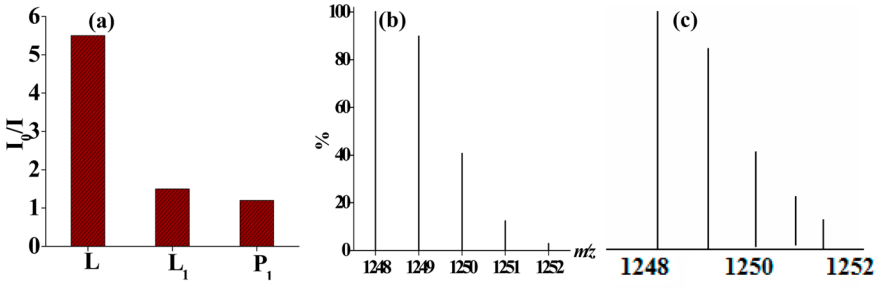

Figure 4. (a) Relative fluorescence intensity for Co^{2+} titration of **L**, $\mathbf{L_1}$, and $\mathbf{P_1}$. ESI mass spectrum showing the isotopic peak pattern of the molecular ion peak for the 1:1 complex formed between **L** and Co^{2+}: (b) experimental and (c) calculated.

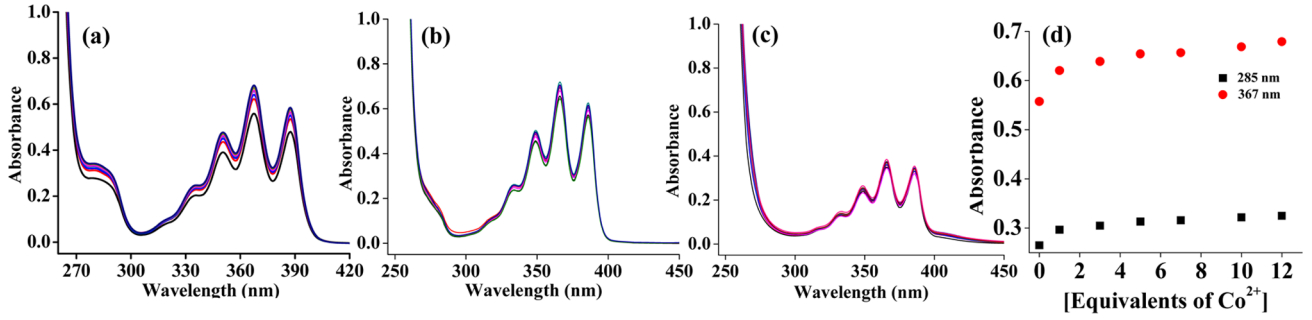

Figure 5. Absorption spectra during the titration with Co^{2+} in ethanol: (a) **L**, (b) $\mathbf{L_1}$, and (c) $\mathbf{P_1}$. (d) Plots of absorbance versus mole ratio of $[Co^{2+}]/[L]$ for different bands.

where the spectrum shows a molecular ion peak at m/z of 1248.6, and the observed isotopic peak pattern supports the presence of Co^{2+} (Figure 4b,c).

Absorption Spectral Studies of L and Reference Molecules with Co^{2+}. In order to confirm the binding of Co^{2+} by **L**, absorption spectral titrations were carried out in ethanol. The isosbestic points observed at 266 and 303 nm suggest the complex formation between **L** and Co^{2+} (Figure 5, Supporting Information, S9). On the other hand, the control molecule, $\mathbf{L_1}$, and the precursor molecule, $\mathbf{P_1}$, did not show any significant change in the absorbance when titrated with Co^{2+}, suggesting that **L** is sensitive and selective toward Co^{2+}.

^{1}H NMR Titration of L with Co^{2+}. During the ^{1}H NMR titration of **L** with Co^{2+}, as the metal ion concentration increases, the anthacenyl -CH_2 peak shifts toward upfield and finally merges with the aromatic proton signals of calix[4]arene. Changes were also observed in the region of the anthracenyl moiety. There are no changes observed in the remaining regions of the spectrum, suggesting that Co^{2+} interacts in the region of the calix[4]arene lower rim and the anthracenyl moiety (Figure 6). Similar titration carried out with $\mathbf{L_1}$ exhibited upfield shift as well as broadening in the anthracenyl -CH_2 peak as the metal ion concentration increases (Supporting Information, Figure S19).

Microscopy Studies. The receptor **L** comprises spherically shaped particles that are well spread all over the mica surface as studied by AFM. However, in the presence of Co^{2+}, these particles seem to merge to result in aggregation, as noticed by their increased size. Thus the size of the particles change from 150 ± 30 nm in pure **L** to 540 ± 80 nm in the presence of Co^{2+} as a result of the metal ion induced aggregation (Figure 7a and b).

Even TEM reveals the formation of spherically shaped vesicular particles over the carbon-coated copper grids for **L**. These spherical vesicular particles vary in size at 500 ± 100 nm. In presence of Co^{2+}, these appear to form chainlike structures as a result of the aggregation promoted by the metal ion coordination (Supporting Information, S11). Thus, both AFM and TEM showed clear-cut changes in the nature and size of

dx.doi.org/10.1021/jo400038x | J. Org. Chem. 2013, 78, 3570−3576

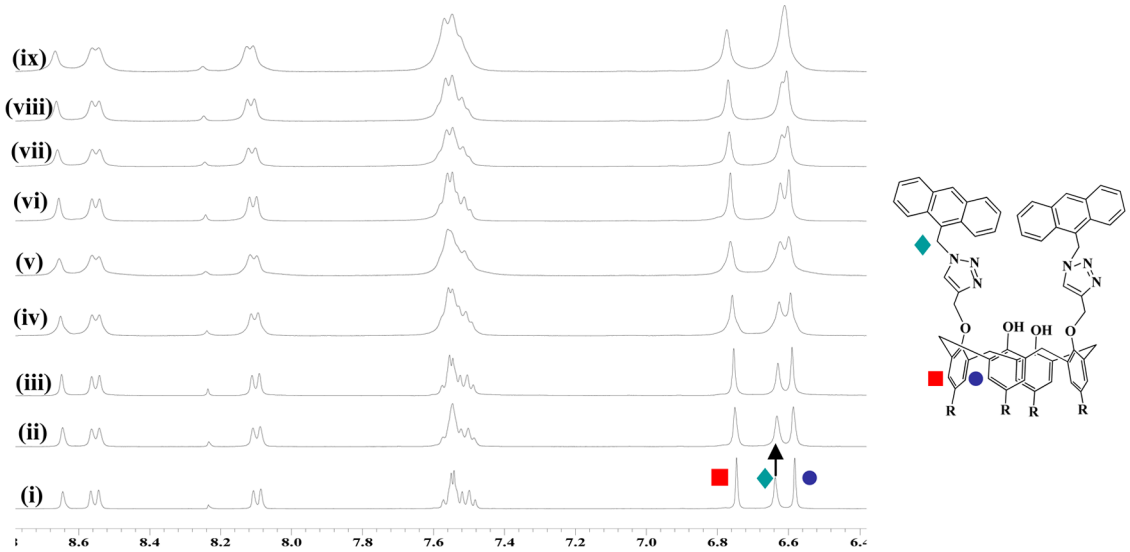

Figure 6. ^{1}H NMR spectra measured during the titration of **L** with Co^{2+} (in DMSO-d_6): (i) 0, (ii) 0.25, (iii) 0.50, (iv) 0.75, (v) 1.0, (vi) 1.5, (vii) 2.0, (viii) 2.5, and (ix) 3.0 equiv.

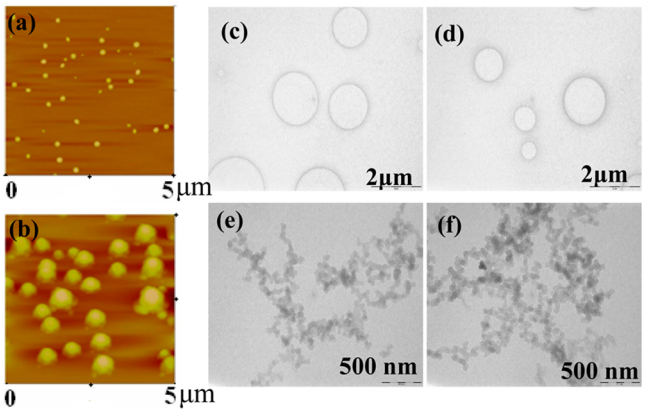

Figure 7. Noncontact mode AFM images of (a) **L** and (b) {**L** + Co^{2+}}. TEM images: (c and d) for **L** and (e and f) for {**L** + Co^{2+}}.

the particles formed from **L** and its Co^{2+} complex (Figure 7c–f).

Structural Features of [CoL] by Density Functional Theory. Computational calculations were carried out using the Gaussian 03 package[8] (Experimental Section) to establish the complexation features of [Co**L**]. In order to do that, initially the crystal structure of **L** was optimized by DFT. The optimized **L** was subjected to the interaction with Co^{2+}, and the corresponding complex was further optimized (Experimental Section and Supporting Information, S12). In the optimized structure of the complex, the Co^{2+} occupies distorted octahedral geometry, by bonding through two each of phoenolate and ether oxygens, and two triazole nitrogens resulting in an N_2O_4 binding core (Figure 8). The geometry optimization of the cobalt complex resulted in conformational changes at the arms in order to accommodate the metal ion. This can be gauged from the dihedral angles of the arm and the distance between the two arms. In the process of optimization of the complex, the anthracenyl moieties were spread out and the nitrogens of the triazole moieties turned to the interior of the calixarene to form a phenolate core to bind Co^{2+}. The highest occupied molecular orbitals (HOMOs) and lowest unoccupied molecular orbitals (LUMOs) were calculated for the **L**, [Co**L**] (Supporting Information, S13) and demonstrated

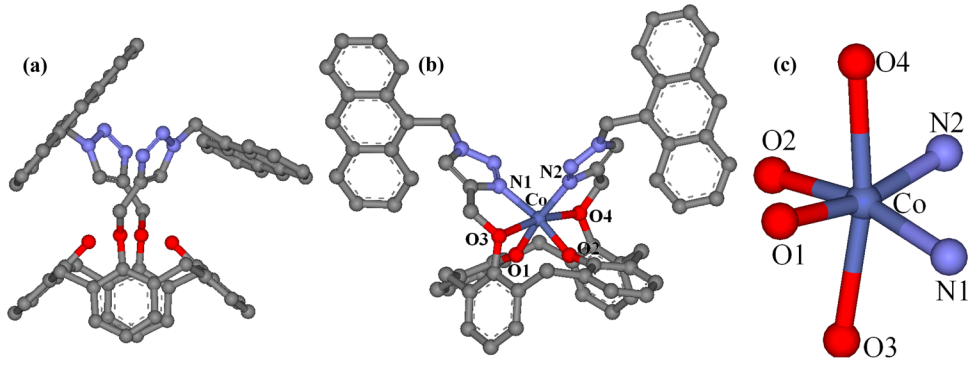

Figure 8. DFT optimized structures: (a) [**L**] and (b) [Co**L**]. (c) An expanded version of the primary coordination sphere of Co^{2+}. The bond lengths (Å) and bond angles (deg) in the coordination sphere are O1–Co = 1.891, O2–Co = 1.890, N1–Co = 1.935, N2–Co = 1.936, O3–Co = 2.271, O4–Co = 2.270; O1–Co–O2 = 85.5, O1–Co–N1 = 91.9, O1–Co–N2 = 165.9, O1–Co–O3 = 83.2, O1–Co–O4 = 88.3, O2–Co–N1 = 165.8, O2–Co–N2 = 92.0, O2–Co–O3 = 88.2, O2–Co–O4 = 83.2, N1–Co–N2 = 93.6, N1–Co–O3 = 77.6, N1–Co–O4 = 110.5, N2–Co–O3 = 110.5, N2–Co–O4 = 77.6, O3–Co–O4 = 168.5.

dx.doi.org/10.1021/jo400038x | J. Org. Chem. 2013, 78, 3570–3576

that the phenolate O^- and triazole N^- core are involved in Co^{2+} binding.

Conformation of the Arms in Presence of Co^{2+} by MD Studies. The conformational aspects of the arms of **L** upon binding Co^{2+} were monitored by analyzing the complex species formed between $\mathbf{L}^{2-}$ and Co^{2+}, viz., [**L**Co] at 0.1-, 1-, and 2-ns simulations carried out by molecular dynamics (Experimental section and Supporting Information, S14). Examination of the cobalt center clearly exhibited six coordinations using the N_2O_4 core that is evolved through these simulations, though the geometry does not fit well with a conventional octahedron. The study clearly showed conformational dynamism of the arms to accommodate the Co^{2+} ion at the lower rim. This can be very well appreciated when the structure of **L** in [**L**Co] is compared with that in the crystal structure. Thus both DFT and MD studies showed coordination around the Co^{2+} to be the same.

Time-Dependent Fluorescence Intensity of L When Titrated with Co^{2+}. As the Co^{2+}-treated **L** solutions left in air showed increase in the fluorescence intensity, a systematic study was carried out to gauge the fluorescence enhancement of these solutions as a function of time by measuring the intensity at different time intervals, viz., 0.5, 1, 3, 6, and 10 h. Initially the fluorescence intensity of **L** decreases as Co^{2+} concentration increases, and when these solutions are left as is, the intensity once again increases as a function of time and by ~10 h the fluorescence intensity is same as that of simple **L**, suggesting oxidative detachment of the cobalt ion (Figure 9).

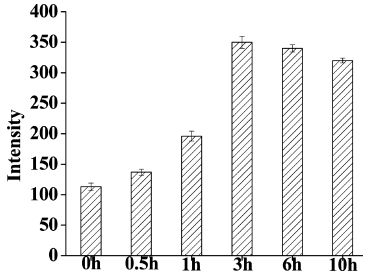

Figure 9. Time-dependent fluorescence intensity of [**L** + 5 equiv Co^{2+}].

Conclusions and Correlations. A new triazole-linked anthracenyl-based 1,3-diconjugate of calix[4]arene (**L**) and two control molecules have been synthesized and were well characterized by various techniques. While the ^{1}H NMR of the receptor **L** supports cone confirmation, this has been proven by establishing the single crystal XRD structure. **L** showed selectivity toward Co^{2+} among 13 biologically and ecologically relevant metal ions, viz., Na^+, K^+, Mg^{2+}, Ca^{2+}, Mn^{2+}, Fe^{2+}, Co^{2+}, Ni^{2+}, Cu^{2+}, Zn^{2+}, Cd^{2+}, Ag^+, and Hg^{2+} as studied by fluorescence and absorption spectroscopy. **L** can detect Co^{2+} down to 55 ppb (0.92 μM), and its fluorescence quenching constant, K_q, is $(4.8 \pm 0.2) \times 10^5$ M^{-1}. Comparison of the fluorescence results of **L** with those of the control, $\mathbf{L}_1$, and precursor, $\mathbf{P}_1$, clearly suggests the necessity of the calix[4]arene platform for the selective detection of Co^{2+} ion. While the Job's plot supported the formation of 1:1 complex between **L** and Co^{2+}, the same has been confirmed by ESI-MS. Both the AFM and TEM showed nanostructural features sufficient enough to differentiate **L** from its cobalt complex, particularly based on the shape and size of the particles. The complexation between **L** and Co^{2+} has been further addressed by computational modeling wherein the Co^{2+} occupies distorted octahedral geometry, by bonding through two phoenolate and two ether oxygens, and two triazole nitrogens to have a N_2O_4 binding core. The hexa-coordination of Co^{2+} has been further confirmed from the analysis of the complex species formed when subjected to the molecular dynamics studies. Thus **L** can be used as selective receptor toward Co^{2+} by fluorescence and nano structural features.

EXPERIMENTAL SECTION

General Information and Materials. Single crystal X-ray diffraction data for **L** were collected at low temperature (160 K). NMR spectra were recorded on a 400 MHz spectrometer. FTIR spectra were recorded from their KBr pellets. HRMS spectra were recorded by Q-TOF using electrospray ionization method.

Fluorescence and Absorption Titrations. Fluorescence emission spectra were measured by exciting the samples at 368 nm, and the emission spectra were recorded in the 378−600 nm range. The bulk solutions of **L** and metal ions were prepared in C_2H_5OH in which 100 μL of $CHCl_3$ was used for dissolving **L**. Bulk solution concentration of **L** and metal ion concentration were maintained at 6×10^{-5} M. All measurements were made in 1-cm quartz cells, and the effective cuvette concentration of **L** was maintained as 5 μM in all of the titrations. During the titration, the concentration of metal ions was varied accordingly in order to result in requisite mole ratios of these to **L** by taking a fixed volume and varying volumes of the solution of the metal ions. The total volume of the solution used for the fluorescence measurements was maintained constant at 3 mL in all the cases by simply adding the requisite volume of ethanol as the making up solvent. In the case of absorption titrations the bulk solutions of **L** and metal ions were prepared in C_2H_5OH in which 100 μL of $CHCl_3$ was used for dissolving **L**. Bulk solution concentration of **L** and metal ion concentration were maintained at 6×10^{-3} M. All measurements were made in 1-cm quartz cells, and the effective cuvette concentration of **L** was maintained as 5 μM in all of the titrations.

Microscopy Studies. The AFM samples of **L** and [**L** + Co^{2+}] were prepared at 6×10^{-5} M concentration in ethanol. The receptor **L** was initially dissolved in 100 μL of $CHCl_3$ and then made up with ethanol to the desired concentration. The stock solutions of these were sonicated for 15 min. A 50−100 μL aliquot was taken from this stock solution to spread over a mica sheet using the drop cast method. The samples were then dried and analyzed by AFM. The TEM samples of **L** and [**L** + Co^{2+}] were prepared at 6×10^{-3} M concentration in ethanol. The receptor **L** was initially dissolved in 100 μL of $CHCl_3$ and then in ethanol. The stock solutions of **L** and [**L** + Co^{2+}] were sonicated for 15 min, after which a 50−100 μL aliquot was taken and spread over the carbon-coated grid using the drop cast method.

Synthesis and Characterization of P_1. A mixture of 9-(chloromethyl)anthracene (1.0 g, 4.41 mmol) and sodium azide (0.43 g, 6.62 mmol) was taken in 20 mL of DMF. The resulting solution was stirred for 12 h at room temperature. After completion of the reaction, water was added to the reaction mixture and extracted with EtOAc (3 × 30 mL), and the resulting extract was washed with water followed by brine solution. A pure product was obtained by evaporating the organic solvent (yield 0.95gm, 92%). ^{1}H NMR ($CDCl_3$, 400 MHz, δ ppm) 5.32 (s, 2H, anthracene-C**H**$_2$), 7.48−7.61 (m, 4H, anthracene-**H**), 8.04 (d, 2H, J = 8.84, anthracene-**H**), 8.28 (d, 2H, J = 8.84, Anthracence-**H**), 8.50 (s, 1H, anthracene-**H**). ^{13}C NMR ($CDCl_3$, 100 MHz, δ ppm): 46.5 (anthracene-**C**H$_2$), 123.7, 125.4, 125.9, 127.0, 129.2, 129.5, 130.9, 131.6 (anthracene-Ar-**C**) . **HRMS**: for $C_{15}H_{11}N_3$: calculated: 233.0953 found: 233.0957 **FTIR** (KBr, cm^{-1}): 2096 (ν_{-N3}), 2968 (ν_{-C-H}).

Synthesis and Characterization of P_2. A mixture of potassium carbonate (5.18 g, 37.34 mmol) and p-*tert*-butylcalix[4]arene (10.0 g, 15.43 mmol) in acetone (200 mL) was stirred at room temperature for 1 h. Propargyl bromide (6.34 g, 53.08 mmol) was added dropwise into the stirred mixture over 30 min. The reaction mixture was refluxed for 24 h and then allowed to cool to room temperature. This was then filtered over Celite to remove insoluble particles and the filtrate was concentrated by a rota-evaporator. A 100 mL of 2 M HCl was added

dx.doi.org/10.1021/jo400038x | J. Org. Chem. 2013, 78, 3570−3576

to the concentrated reaction mixture and the product was extracted with dichloromethane (3 × 100 mL). The combined organic extracts were successively washed with water and brine (100 mL), dried over anhydrous Na_2SO_4, filtered and evaporated to dryness *in vacuo*. The crude product was recrystallized from CH_2Cl_2/CH_3OH to afford **2** as a white solid (Yield, 82%). ^{1}H NMR ($CDCl_3$, 400 MHz, δ ppm): 7.07 (s, 4H, Ar-**H**), 6.73 (s, 4H, Ar-**H**), 6.50 (s, 2H, **OH**), 4.74 (d, J = 2.4 Hz, 4H, OC**H**$_2$), 4.37 (d, J = 13.4 Hz, 4H, ArC**H**$_2$Ar), 3.33 (d, J = 13.4 Hz, 4H, ArC**H**$_2$Ar), 2.54 (t, J = 2.4 Hz, 2H, C≡C**H**), 1.30 (s, 18H, (C**H**$_3$)$_3$), 0.90 (s, 18H, (C**H**$_3$)$_3$); ^{13}C NMR ($CDCl_3$, 100 MHz, δ ppm): 31.1 (-C(C**H**$_3$)$_3$), 31.9, 32.2 (-**C**(CH$_3$)$_3$), 34.0, 34.0 (Ar-C**H**$_2$–Ar), 63.5 (-O-C**H**$_2$), 76.5 (-C≡C**H**), 78.9 (-**C**≡CH), 125.2, 125.7, 128.2, 132.7, 141.8, 147.4, 149.6, 150.5 (Ar-**C**). **HRMS** m/z Calcd for $C_{50}H_{60}O_4$: 725.4570, Found 725.4565 **FTIR** (KBr, cm^{-1}): 2968 (ν_{-C-H}), 3308 (ν_{-C-H}), 3505 (ν_{-OH}).

Synthesis and Characterization of L. A mixture of calix[4]-dipropargyl, $\mathbf{P_2}$ (0.6 g, 0.4 mmol), and 9-(azidomethyl)anthracene (0.48 g, 0.9 mmol) were taken in 20 mL of {dichloromethane (5 mL)/*tert*-butanol (5 mL)/water (10 mL)}. To this were added $CuSO_4{\cdot}5H_2O$ (0.082 g, 0.016 mmol) and sodium ascorbate (0.130 mg, 0.066 mmol). The resulting reaction mixture was stirred for 12 h at room temperature. Upon completion of the reaction as monitored by TLC, the organic layer was separated, and the aqueous layer was extracted with dichloromethane (2 × 50 mL). The combined organic layers was washed with brine (2 × 50 mL) and dried over anhydrous Na_2SO_4, the mixture was filtered, and the solvent was removed under vacuum The crude product was purified by column chromatography using EtOAc/petroleum ether (2:8) (yield 0.55 g, 60%). Pale yellow crystalline solid, mp 285−288 °C. ^{1}H NMR ($CDCl_3$, 400 MHz, δ ppm): 0.79 (s, 9H, -C(C**H**$_3$)), 1.27 (s, 9H, -C(CH$_3$)), 2.81 (d, 4H, Ar-C**H**$_2$eq-Ar, J = 12.8), 3.62 (d, 4H, Ar-C**H**$_2$eq-Ar, J = 12.8), 4.80 (s, 4H, -O-C**H**$_2$), 6.30 (s, 4H, anthracene-CH$_2$-triazole), 6.47 (s, 4H, Ar-**H**), 6.80 (s, 4H, Ar-**H**), 7.22 (s, 2H, triazole-H), 7.41−7.46 (m, 8H, anthracenyl-**H**), 7.92−7.95 (m, 4H, anthracenyl-**H**), 8.08 − 8.11 (d, 4H, anthracenyl-**H**, J = 9.2), 8.36 (s, 2H, anthracenyl-**H**). ^{13}C NMR ($CDCl_3$, 100 MHz, δ ppm): 30.9, 31.1 (-C(**C**H$_3$)$_3$), 31.6, 31.9 (-**C**(CH$_3$)$_3$), 33.9, 33.9 (Ar-**C**H$_2$-Ar), 47.0 (anthracence-**C**H$_2$-triazole), 69.6 (Ar-**C**H$_2$-triazole), 122.8, 123.1, 123.4, 125.0, 125.5, 125.5, 127.4, 127.7, 129.7, 130.2, 130.7, 131.2, 132.2, 141.7, 144.5, 147.3, 149.6, 149.9 (Ar-**C**). HRMS for $C_{80}H_{83}O_4N_6$: calcd 1191.6476, found 1191.6536. FTIR (KBr, cm^{-1}): 3018 (ν_{-C-H}), 3428 (ν_{-OH}).

Synthesis and Characterization of $\mathbf{L_1}$. A mixture of the mono propargyl derivative of *p*-*tert*-butylphenol (0.2 g, 1.0 mmol) and 9-(azidomethyl)anthracene (0.32 g, 1.3 mmol) were taken in 20 mL of {dichloromethane (5 mL)/*tert*-butanol (5 mL)/water (10 mL)}. To this solution were added $CuSO_4{\cdot}5H_2O$ (0.054 g, 0.2 mmol) and sodium ascorbate (0.88 mg, 0.43 mmol). The remainder of the procedure including purification is the same as that given for **L** (yield 0.3 g, 66%): a straw yellow crystalline solid with mp 180−185 °C. ^{1}H NMR ($CDCl_3$, 400 MHz, δ ppm): 1.24 (s, 9H, C(C**H**$_3$)$_3$), 4.99 (s, 2H, -OC**H**$_2$), 6.54 (s, 2H, anthracene-C**H**$_2$), 6.78 (s, 2H, Ar-**H**, J = 2.16), 6.80 (s, 2H, Ar-**H**, J = 2.20), 7.51−7.62 (m, 4H, anthracene-**H**), 8.07 (d, 2H, anthracene-**H**, J = 5.2), 8.3 (d, 2H, anthracene-**H**, J = 5.1), 8.58 (s, 1H, triazole-**H**). ^{13}C NMR ($CDCl_3$, 100 MHz, δ ppm): 31.6 (-C(**C**H$_3$)$_3$), 34.2 (-**C**(CH$_3$)$_3$), 46.7 (triazole-**C**H$_2$-anthracene), 62.2 (-O-**C**H$_2$-Ar), 114.3, 122.5, 123.1,123.8, 125.6, 126.3, 127.9, 129.7, 130.1, 130.9, 131.6, 144.0, 144.5, 156.0 (Ar-**C**). HRMS for $C_{28}H_{28}ON_3$: calcd 422.2232, found 422.2221, **FTIR** (KBr, cm^{-1}): 1966 ($\nu_{-C=C}$),3019 (ν_{-C-H}).

Computational Methods. The computational calculations were carried out to find the mode of complexation of Co^{2+} with **L**. As the formation of 1:1 {LCo} complex species was established by the ESI MS and were also supported by the other spectroscopic techniques, the 1:1 **L**:Co^{2+} complex species were optimized by using the Gaussian 03 package.[8] The initial model for **L** was taken from the crystal structure reported in this paper. In order to reduce the computational times, before optimization, the **L**′ was made simply by replacing each of the *tert*-butyl group of **L** by a hydrogen. The **L**′ thus obtained was optimized by going through PM3 → HF/STO-3G → HF/3-21G → HF/6-31G → B3LYP/3-21G → B3LYP/6-31G in a cascade manner, and the complex was optimized using B3LYP/6-31G(d,p). The output obtained at every stage was given as the input for the next higher level of calculations. In order to make the cobalt complex, [**L**′(Co)], the phenolic OH groups were deprotonated and the resulting $(\mathbf{L}')^{2-}$ was used for further studies. The complex formation was initiated by placing the Co^{2+} far away from both arms of $(\mathbf{L}')^{2-}$ in such a way that the phenolate-O, triazole-N atoms are pointed toward the cobalt center. The molecular orbital's (MOs) were generated by using Gauss view software.

Molecular Dynamics Studies. The DFT optimized structure of **L** at B3LYP/-6-31G was used as the starting model. Thus the interactions present between **L** and the Co^{2+} were modeled by carrying out molecular dynamics (MD) simulations under vacuum using the GROMOS96 43a1 force field available with the GROMACS 4.0.5 software package.[9a,b] The force fields were generated for **L** using PRODRG server.[9c] The charges were calculated for using ChelpG[9d] method (available with G03) and were added to the topology file that was generated by PRODRG. The simulations were carried out for 2 ns with the system where one of the complex, **L** plus 10 copies of Co^{2+} were taken in a cubic box. The total contents of the system were energy minimized for ∼2,000 steps with the Steepest Descent (SD) method.[9e] Then the whole cubic box was allowed for simulation under NVT condition (T = 300 K) with the equation of motion being integrated by the leapfrog algorithm with a step size of 2 fs. At the time of carrying out the computations **L** and the Co^{2+} were coupled separately to v-rescale temperature bath. The electrostatic interactions were calculated using the particle Mesh Ewald summation method.[9f] All bond lengths of **L** were constrained using the LINCS[9g] algorithm.

NMR Titration. The binding of Co^{2+} by **L** was further conformed by ^{1}H NMR titration. The receptor **L** (0.01 M) was dissolved in 0.4 mL of DMSO-d_6, and the ^{1}H NMR spectrum was recorded in the absence of metal ion. Metal ion titrations were carried out by adding different volumes of $Co(ClO_4)_2{\cdot}6H_2O$ (0.1 M) solutions, viz., 5, 10, 20, 30, 40, 60, 80, and 120 μL to the solution of **L**, which resulted in a [Co^{2+}]/[**L**] mole ratio of 0 to 3

■ ASSOCIATED CONTENT

Ⓢ Supporting Information

^{1}H and ^{13}C NMR, mass spectral data of $\mathbf{P_1}$, $\mathbf{P_2}$, **L**, and $\mathbf{L_1}$; fluorescence and absorbance spectra of all metal ions; ^{1}H NMR titration of $\mathbf{L_1}$ with Co^{2+}; crystal data for **L**; DFT and MD data for **L** and [Co**L**]. This material is available free of charge via the Internet at http://pubs.acs.org.

■ AUTHOR INFORMATION

Corresponding Author

*E-mail: cprao@iitb.ac.in.

Notes

The authors declare no competing financial interest.

■ ACKNOWLEDGMENTS

C.P.R. acknowledges financial support from DST, CSIR, and DAE-BRNS. V.V.S.M. and V.K.H. acknowledge CSIR for SRF, and K.T. acknowledges UGC for SRF. We thank Ms. Radhika Anaredy for help obtaining spectra. We also acknowledge FIST (Physics)-IRCC central SPM facility of IIT Bombay for AFM studies and CRNTS (SAIF) of IIT Bombay for TEM facility.

■ REFERENCES

(1) (a) Barceloux, D. G. *Clin. Toxicol.* **1999**, *37*, 201. (b) Pais, I.; Jones, J. B. *The Handbook of Trace Elements*, St. Lucie Press: Boca Raton, FL, 1997. (c) Agency for Toxic Substances and Disease Registry (ATSDR), Toxicological Profile for Cobalt, Public Health Service, U.S. Department of Health and Human Services: Atlanta, GA, 2004. (d) Abebe, F. A.; Eribal, C. S.; Ramakrishna, G.; Sinn, E. *Tetrahedron Lett.* **2011**, *52*, 5554.

(2) Gupta, V. K.; Jain, A. K.; Khayat, M.; Bhargava, S. K.; Raisoni, J. R. *Electrochemica Acta* **2008**, *53*, 5409.
(3) (a) Little, C.; Aakre, S. E.; Rumsby, M. G.; Gwarsha, K. *Biochem. J.* **1982**, *207*, 117. (b) Dennis, M.; Kolattukudy, P. E. *Proc. Natl. Acad. Sci. U.S.A.* **1992**, *89*, 5306. (c) Maret, W.; Vallee, B. L. *Methods Enzymol.* **1993**, *226*, 52. (d) Walker, K. W.; Bradshaw, R. A. *Protein Sci.* **1998**, *7*, 2684. (e) Okamoto, S.; Eltis, L. D. *Metallomics* **2011**, *3*, 963.
(4) Gharehbaghi, M.; Shemirani, F.; Farahani, M. D. *J. Hazard. Mater.* **2009**, *165*, 1049.
(5) Memon, S.; Yilmaz, M. *J. Mol. Struct.* **2001**, *595*, 101.
(6) (a) Au-Yeung, H. Y.; New, E. J.; Chang, C. J. *Chem. Commun.* **2012**, *48*, 5268. (b) Maity, D.; Govindaraju, T. *Inorg. Chem.* **2011**, *50*, 11282. (c) Maity, D.; Kumar, V.; Govindaraju, T. *Org. Lett.* **2012**, *14*, 6008. (d) Yao, Y.; Tian, D.; Li, H. *ACS Appl. Mater. Interfaces* **2010**, *2*, 684. (e) Lin, W.; Yuan, L.; Long, L.; Guo, C.; Feng, J. *Adv. Funct. Mater.* **2008**, *18*, 2366. (f) Zhen, S. J.; Guo, F. L.; Chen, L. Q.; Li, Y. F.; Zhang, Q.; Huang, C. Z. *Chem. Commun.* **2011**, *47*, 2562. (g) Mameli, M.; Lippolis, V.; Caltagirone, C.; Capelo, J. L.; Faza, Q. N.; Lodeiro, C. *Inorg. Chem.* **2010**, *49*, 8276. (h) Kumar, P.; Shim, Y.−B. *Talanta* **2009**, *77*, 1057.
(7) (a) Pathak, R. K.; Dikundwar, A. G.; Guru Row, T. N.; Rao, C. P. *Chem. Commun.* **2010**, 4345. (b) Joseph, R.; Rao, C. P. *Chem. Rev.* **2011**, *111*, 4658.
(8) Pople, J. A. et al. *Gaussian 03, revision C.02*; Gaussian, Inc.: Wallingford, CT, 2004 (complete ref in Supporting Information, S15).
(9) (a) Hess, B.; Kutzner, C.; van der Spoel, D.; Lindahl, E. *J. Chem. Theory Comput.* **2008**, *4*, 435. (b) van der Spoel, D.; Feenstra, K. A.; Hemminga, M. A.; Berendsen, H. J. C. *Biophys. J.* **1996**, *71*, 2920. (c) Schuettelkopf, W.; van Aalten, D. M. F. *Acta Crystallogr.* **2004**, *D60*, 1355. (d) Brenneman, C. M.; Wiberg, K. B. *J. Comput. Chem.* **1990**, *11*, 36. (e) Deift, P.; Zhou, X. *Ann. Math.* **1993**, *137*, 295. (f) Darden, T.; York, D.; Pedersen, L. *J. Chem. Phys.* **1993**, *98*, 10089. (g) Hess, B.; Bekker, H.; Berendsen, H. J. C.; Fraaije, M. J. G. E. *J. Comput. Chem.* **1997**, *18*, 1463.